npj | Flexible Electronics

www.nature.com/npjflexelectron

ARTICLE OPEN

Check for updates

Flexible and transparent piezoelectric loudspeaker

M. Shehzad[1,2], S. Wang[1] and Y. Wang[1]✉

The simple structure of flexible piezoelectric polymers implies promise innumerous applications, such as transparent loudspeakers. In this study, we fabricated and characterized a prototype loudspeaker device. The loudspeaker was fabricated using a straightforward method of sandwiching a film of copolymer blend between a pair of flexible ITO substrates, which served as top and bottom electrodes. The dependence of acoustic properties of the devices was investigated in accordance with d_{33} and piezoresponse force microscopy (PFM). In this study, we examine the sound pressure level (SPL) and sound intensity (SI) of devices featuring $0.5 \le \alpha \le 0.9$ blends, with an active area of 6.5 cm × 5 cm at 100 Vpp applied voltage. Here we report SPL of 96 dB and SI of 3.98 m Wm^{-2} for an $\alpha = 0.7$ blend at 100 Vpp. Our results are helpful in developing flexible, transparent piezoelectric polymers and in the development of lightweight, transparent loudspeaker devices.

npj Flexible Electronics (2021)5:24 ; https://doi.org/10.1038/s41528-021-00121-z

INTRODUCTION

Since the discovery of piezoelectric properties in PVDF-based polymers, scientists and designers have been exploring pathways to incorporate transparent piezoelectric devices in the fast-growing smart-device culture of the modern age[1]. PVDF polymers are lightweight, transparent, and can be processed using simple techniques[2–5]. PVDF-based polymers contain good ferroelectric, pyroelectric, and piezoelectric properties, making them ideal candidates for transparent sensors and actuators. Researchers are also trying to investigate the electroacoustic properties of such polymers. One such use of that takes advantage of the reverse piezoelectric effect of such materials is a transparent thin-film loudspeaker. Unlike conventional magnetic loudspeakers that exhibit high acoustic performance at low voltage, current thin-film loudspeakers are mostly driven at high voltage. The higher operational voltage of such piezoelectric materials restricts their widespread application in many existing technologies. However, there are some limitations of the conventional loudspeakers. The conventional loudspeakers are heavy in weight and based on electric coils.

Although conventional magnetic loudspeakers are ubiquitous in audio applications, the form and composition of such devices preclude their use in many of the emerging smart devices that often require lightweight, portable, and transparent components. Unlike their opaque and heavy piezoelectric ceramic counterparts, polymeric piezoelectric loudspeakers are simple in structure and easy to fabricate[6–9]. These loudspeakers are so thin that they can be pasted on touch screens to produce acoustic vibrations without sacrificing screen visibility, and without the need for hazardous magnetic field emission[10–12].

PVDF-based polymeric loudspeakers were introduced in 1975[13]. A multiresonance bimorph actuator developed on a polyester film substrate for loudspeaker application was fabricated by Ohga et al. in 1983[14]. Later, a researcher in 2003 compared the acoustic efficiency of PVDF-based loudspeakers using different electrode materials[15]. Multilayer PVDF film-based bimorph loudspeakers were fabricated by Bailo et al. in 2003[16].

The basic property of ferroelectric polymers that enables their applications in functional materials is the presence of switchable polarization and their domain boundary structures. Ferroelectric and electroresistive memories, electrostriction, and transduction properties are also associated with polarization switching behavior[17–21]. The energy harvesting, electrostriction, and transduction properties of PVDF-based ferroelectric polymers are very good compared to other ferroelectric materials. Similarly, other smart devices fabricated out of these polymers also have excellent sensing properties[22–26]. The piezoelectric properties of PVDF-based polymer blends mainly depend on the percentage of the beta phase. Recent research has shown that ferroelectric blends enable tuning of the structural properties of these materials, with good results in increasing the beta phase percentage[27]. Gomes et al. 2010 investigated the role of beta phase content and degree of crystallinity on piezoelectric and ferroelectric properties of PVDF-based polymers[28]. He concluded that the stretching ratio and temperature deeply influence the transformation of the nonpolar alpha phase to the polar beta phase. He also reported the influence of beta phase content on the piezoelectric coefficient (d_{33}). Recently, Alexandre De. Neef et al. 2020 studied the enhancement of beta phase crystallization of melt-processed PVDF blends with PMMA copolymers, reporting a piezoelectric coefficient (d_{33}) up to 11 pCN^{-1} by just blending the PVDF with PMMA. His report showed that blending PVDF with PMMA in a 3:2 ratio followed by a rapid quench resulted in an increased beta phase[29]. Hence, by just blending and poling of PVDF blends we can enhance the percentage of the beta phase, piezoelectric properties, and electroacoustic properties.

In this research, we investigate the acoustic properties of P(VDF-TrFE) and P(VDF-TrFE-CTFE) blends in which we have already achieved the beta phase by blending the definite proportion of copolymer into terpolymer[30]. The nonpolar alpha phase gradually and slowly converted to the polar beta phase. The copolymer is blended with terpolymer in a proportion to enhance the beta phase reflection by electric and thermal poling. The films are fabricated by the lab-made applicator by using the electronics assembly of a scanner and by pushing the scan button we dispensed the thin films shown in Supplementary Fig. 1a. Our process yields films with a thickness on average 12 µm, as also shown in thickness profiles in Supplementary Fig. 1b.

[1]School of Materials Science and Engineering, Nanjing University of Science and Technology, Nanjing, Jiangsu, China. [2]School of Chemical and Materials Engineering, National University of Sciences and Technology (NUST) H-12, Islamabad, Pakistan. ✉email: yjwang@njust.edu.cn

Published in partnership with Nanjing Tech University

npj nature partner journals

The 6.5 cm × 5 cm piezoelectric loudspeaker device is prepared by sandwiching the polymer blends between a pair of ITO electrodes, as shown schematically in Fig. 1. Unlike previous studies, we have fabricated our loudspeakers without sandwiching any paper between the ITO electrodes. While the addition of paper to the laminate will reduce the chance of dielectric breakdown, such layers reduce device transparency[31]. The remnant polarization (*Pr*) and hysteresis loop were characterized to visualize the beta phase enhancement. Furthermore, the sound was recorded for moving the microphone towards the sound and moving the microphone away from the sound. Furthermore, the sound was also recorded with continuously poling at the different electric fields, and SPL was measured with the help of sound intensity (SI) and sound pressure (Pa). We have achieved higher SPL for our devices than that reported in the literature (91 dB SPL) while retaining a higher degree of transparency[32].

RESULTS

Fourier transform infrared and UV-Vis spectroscopy

Fourier transform infrared spectroscopy (FTIR) shows the reflection peaks of polymer blends carried out from 600 to 1800 cm^{-1} (Fig. 2). The neat copolymer has some gamma phase while the neat terpolymer contains mostly nonpolar alpha phase, as shown in Fig. 2a. The beta phase in the FTIR spectra can be seen as the resultant reaction of alpha and gamma peaks arising from the blending of the two different polymers. The intensity of beta peaks increases with increasing the copolymer content (*α*). Therefore, the beta phase reflection peak of $\alpha = 0.5$ to 0.9 blends is higher than the rest of the polymer blends, as shown in Fig. 2b.

Figure 2c, d show the ultraviolet-visible (UV-Vis) transmission and reflection spectra of polymer blends compositions. The $\alpha = 0.9$ blend is more transparent than the rest of the polymer blends, as seen by a higher transmission and lower absorption than the other blend compositions. Figure 2e–j shows the 2D contour graphs of percentage transmittance and percentage absorbance for different polymer blends. Although the $\alpha = 0.9$ has the highest transparency, we choose to develop our loudspeaker device using an $\alpha = 0.7$ blend because of its high transduction properties over the range of electric field excitation chosen.

Supplementary Fig. 1c shows the XRD curves of polymer blends in which the nonpolar peaks at $2\text{-}\Theta = 18.4°$ and the polar beta peaks at 20° are clearly visible. The trend of beta reflection increasing with increasing terpolymer composition is similar in both FTIR and XRD curves.

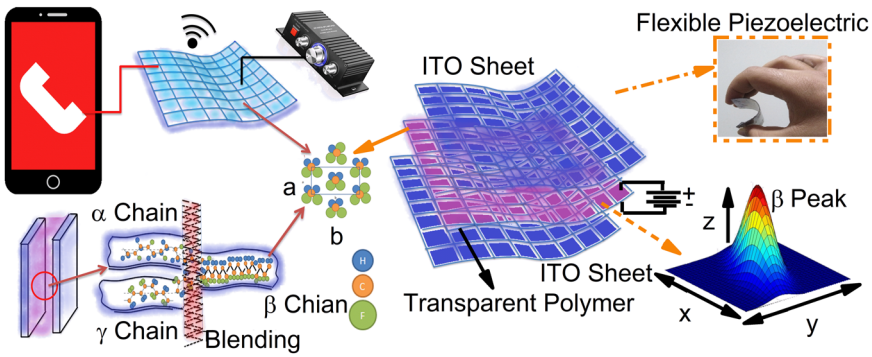

Fig. 1 Piezoelectric transducer. The schematic depiction of a flexible and transparent piezoelectric loudspeaker made by sandwiching transparent polymers between two ITO electrodes. Also shown is the backbone beta chain structure of P(VDF-TrFE), synthesized as a result of a reaction of alpha and gamma chains of two different polymers during blending.

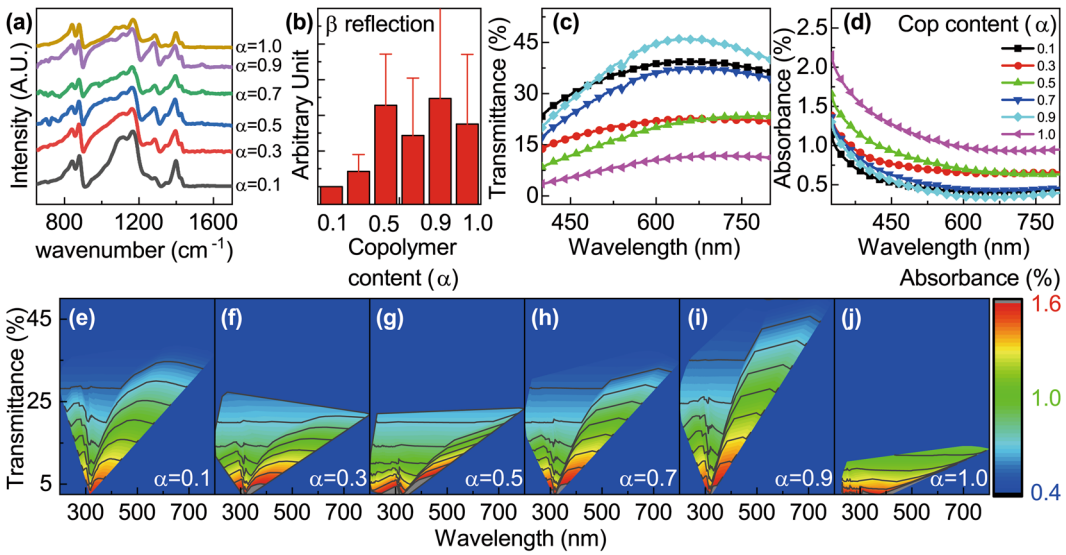

Fig. 2 FTIR and UV-Vis Spectroscopy. a FTIR peaks. **b** Intensity of beta reflection peaks. **c** Percentage of transmittance. **d** Percentage of absorption. **e–j** 2D contour graphs of percent transmittance and percent absorbance of transparent transducers made up of polymer blends. Error bars = standard deviation ($n = 6$).

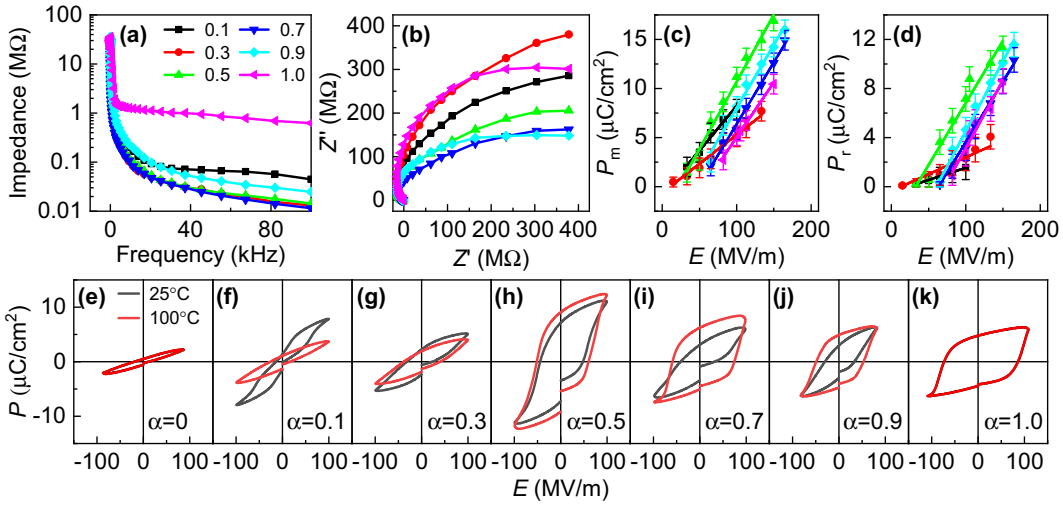

Fig. 3 Dielectric properties and polarization electric field (P-E) hysteresis loop comparison. a Impedance graph. **b** Cole-Cole graph. **c** Maximum polarization (*Pm*) vs electric field *E* (MVm^{-1}) graph. **d** Remnant polarization (*Pr*) vs electric field *E* (MVm^{-1}) graph. **e**–**k** PE comparison graphs of $\alpha = 0$, 0.1, 0.3, 0.5, 0.7, 0.9, and 1.0 blend respectively. Error bars: **a**, **b**, **c**, **d** = standard deviation ($n = 6$), **e**, **f**, **g**, **h**, **i**, **j**, **k** = standard deviation ($n = 7$).

Dielectric and polarization hysteresis loop comparison

Figure 3 shows the dielectric properties and PE hysteresis loop graphs of polymer blends at various electric fields. The maximum polarization (*Pm*) for P(VDF-TrFE) is higher than the P(VDF-TrFE-CTFE) due to the inherent beta phase. The terpolymer is nonpolar and therefore the *Pm* is slightly lower and the PE loop trend is almost linear. The copolymer also has high *Pr*. The *Pm* to *Pr* ratio is an important factor to describe the PE hysteresis loop behavior. The terpolymer tends to have a lower *Pr* and therefore a higher *Pm* to *Pr* ratio than the other polymer blends. As shown in the impedance curves of Fig. 3a, the impedance of the copolymer is higher than that of the relaxor terpolymers. However we have observed a sharp increase due to the antiferroelectric properties of polymer blends (see Supplementary Fig. 1d, e). The impedance values of the $0.5 \le \alpha \le 0.9$ blends are slightly lower than the other blend composition, with a notable minimum for the $\alpha = 0.7$ blend. Therefore, we can correlate the dependence of acoustic properties of these blends with impedance values. The blend which may have less impedance values can be fabricated as a primitive piezoelectric loudspeaker at a higher electric field. Consequently, from the above figures, the trend of $\alpha = 0.5$ to 0.9 is showing the prominent normal ferroelectric behavior which eventually leads to the enhancement in piezoelectric coefficient with the increment of its crystalline characteristics.The Cole-Cole graph shown in Fig. 3b shows a similar trend of lower impedance values for $\alpha = 0.7$ blends.

The line graph of *Pm* vs electric field *E* (MVm^{-1}) (Fig. 3c) shows that the *Pm* of $0.5 \le \alpha \le 0.9$ blends is slightly higher than the rest of the polymer blends. This is due to the dominance of the antiferroelectric behavior of these blends. The $\alpha = 0.1$ to 0.3 are also antiferroelectric polymers but they show the double hysteresis loop only in a lower electric field. The $\alpha = 0.5$ to 0.9 blends show prominent antiferroelectric double hysteresis loops over a wide range of electric fields. The *Pr* of $\alpha = 0.5$ to 0.9 blend is also low at the lower electric field but it shows a linear increase after 50 MVm^{-1} (Fig. 3d).

The effect of thermal poling is shown in the PE hysteresis loops at 25 and 100 °C, shown in Fig. 3e–k. Interestingly, the $\alpha = 0.5$ to 0.9 blends show an increase in *Pm* after thermal poling at 100 °C, but the effect of poling for lower blends (i.e., $\alpha = 0.1$ and 0.3) is negligible. We can correlate the change in polarization with temperature and piezoelectric enhancement upon thermal poling at 100 °C. We concluded that the enhancement in polarization plays a vital role to increase the d_{33} by thermal poling. The increment of polarization with thermal poling at 100 MVm^{-1} is also shown in Supplementary Fig. 1f.

Piezoresponse force microscopy (PFM)

Piezoresponse force microscopy (PFM) was used to characterize the polymer blends at room temperature (Fig. 4). The samples were poled at an electric field of 100 MVm^{-1} prior to PFM characterization. As shown in Fig. 4a, samples were probed for response in phase with electric poling. The micrographs of Fig. 4b show that the size of the ferroelectric domain gradually increases and decreases from $\alpha = 0.1$ to 0.9 blends. The PFM phase hysteresis loop for extended and retracted states was measured for $\alpha = 0.1$ to 1.0 blends, as shown in the phase (degree) vs tip bias (*V*) and amplitude vs tip bias (*V*) curves of Fig. 4c.

The PFM phase images show the contrast of domain boundaries which are distinguished as domains with upward and downward polarizations with respect to the cantilever direction. We observed an enhancement in polarization switching behavior for $\alpha = 0.1$ to 1.0 sample by locally poling the blends at negative and positive biases. By decreasing the applied field from maximum to zero polarization we observed the phase changes shown in the comparison graph in Fig. 4d, e. In the hysteresis graphs, we applied −10 to +10 V for the first loop, and another loop was observed when applying electric field from +10 to −10 V. The average domain and crystallite size is represented in Supplementary Fig. 1g which shows the increase and decrease in the average domain size of polymer blends by increasing the copolymer content (α). The refined domains of $\alpha = 0.5$ to 0.9 blends help to perform a more efficient response to the input audio signal (Vpp).

Sound pressure level (SPL) and d_{33} comparison

The SPL was measured for loudspeaker devices fabricated from samples spanning all the polymer blends according to ISO 3382-1:2009(E)[33] standard, as illustrated in Fig. 5a. The sound emitted by the devices was captured using Smaart V7™ software. The test sample was mounted in a lab-based test bed that holds the 6.5 cm × 5 cm rectangular and transparent piezoelectric device in a vertical position, as illustrated in Fig. 5a–c. The polymer blends were held in a vertical position and a sensitive microphone was placed at 1 m distance according to the ISO standard. A function

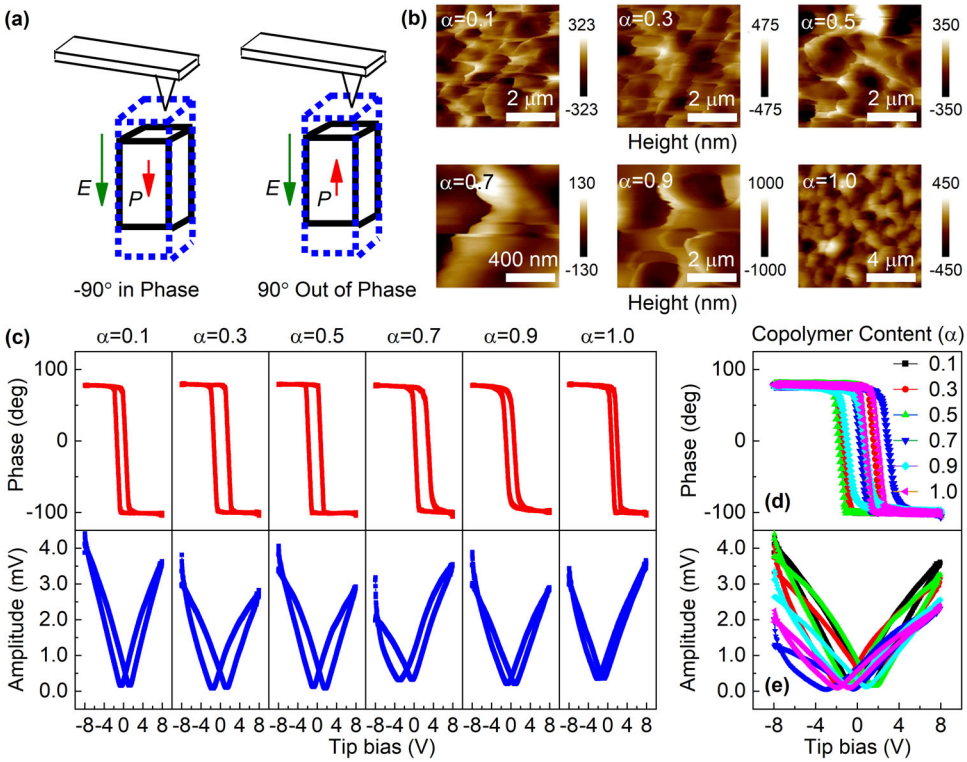

Fig. 4 Piezoresponse force microscopic analysis. a Cantilever position and in-phase and out-of-phase schematic description during testing. **b** Piezoresponse force microscopy (PFM). **c** Phase (degree) and amplitude vs tip bias (*V*) hysteresis. **d**, **e** Comparison between piezoresponse force microscopy hysteresis loops and amplitude graphs of $\alpha = 0.1$, 0.3, 0.5, 0.7, 0.9, and 1.0 blends respectively. Error bars = standard deviation ($n = 6$).

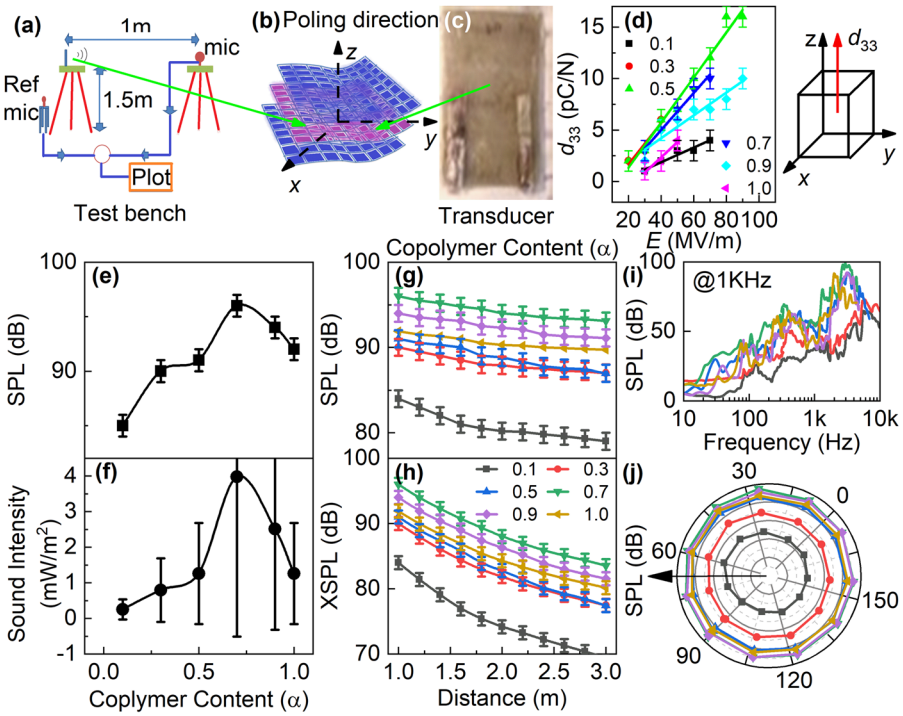

Fig. 5 Transduction and piezoelectric properties. a Schematics of the test configuration for acoustic measurement of the transparent thin films according to ISO standard. **b** Poling direction of the device. **c** Image of actual transducer laminate. **d** Piezoelectric coefficient of polymer blends. **e** SPL comparison at 1 m distance at 100 Vpp. **f** Sound intensity (Wm^{-2}) graph at 1 m distance at 100 Vpp. **g** SPL graph with respect to distance. **h** The inverse law for attenuation of sound with respect to distance. **i** SPL with respect to the sampling frequency at 1 kHz. **j** Polar graph of SPL of polymer blends at 1 kHz. Error bars = standard deviation ($n = 6$).

generator drives the devices at 1 kHz and its output signal was amplified at a high electric field (i.e., 100 Vpp).

The SPL is measured relative to a reference signal, Pref. SPL can therefore be defined as

$$\mathrm{SPL} = 20 * \mathrm{Log}_{10}(\mathrm{P_A}/\mathrm{P_{ref}}) \quad (1)$$

Where P_A is the root mean square (RMS) value of the sound pressure and $P_{ref} = 20$ μPa is the reference pressure for SPLs in the air in Eq. 1, measured at a fixed distance from the source, as prescribed in the ISO test standard.

Nominally, the SPL should follow an inverse square relation with respect to distance. This relationship can be represented as Eq. 2

$$\mathrm{XSPL}(dB) = \mathrm{SPL} - 20 * \mathrm{Log}_{10}(\mathrm{R_2}/\mathrm{R_1}) \quad (2)$$

where XSPL (*dB*) is the theoretical SPL at X distance, SPL is sound pressure level at a particular distance, R_1 is the initial distance from the source, and R_2 is the final distance from the source.

Figure 5d shows the piezoelectric coefficient (d_{33}) of blended polymer with different copolymer contents with respect to the applied voltage. The d_{33} of $\alpha = 0.1$ to 1.0 blends are showing a sharp increase and decrease with the addition of further copolymer content. Hence the d_{33} of $\alpha = 0.5$ and 0.7 blends show the sharp increase in trend at a higher electric field. The SPL in Fig. 5e shows a general increase with respect to blend percent with a notable peak for the $\alpha = 0.7$ and decreases with more copolymer content. As shown in Supplementary Fig. 1h, we obtained a d_{33} value of 15 $\mathrm{pCN^{-1}}$ for the $\alpha = 0.7$ blend—the highest reported value obtained to date for transparent piezoelectric polymer blends. There is a strong correlation between the polarization (*Pm*, *Pr*) and SI of these polymer blends. The *Pm* and *Pr* of $\alpha = 0.5$ to 0.9 are higher than other blends (see Fig. 3) and these blends also exhibit excellent crystalline properties (see Fig. 2). The sound power is translated in the terms of SI ($\mathrm{Wm^{-2}}$). From Fig. 5f the maximum SI was recorded by $\alpha = 0.7$ blend while applying the high output audio signal. The maximum SI is recorded as 3.98 m $\mathrm{Wm^{-2}}$ for $\alpha = 0.7$ blend.

The sharp increase in SPL for the $\alpha = 0.7$ blend is due to an enhancement in the beta phase after blending. Figure 5g shows the damping of sound by moving the detector away from the source. The maximum SPL for $\alpha = 0.7$ and 0.9 is measured as 96 and 94 dB respectively when placing the detector at a 1 m distance from the transducer. In order to confirm the intensity of sound, we have also performed the thermography test that indicates the loudness of sound emitted from the loudspeaker screens shown in Supplementary Fig. 2. In addition to this, Fig. 5h–j shows the inverse law for attenuation of sound with respect to distance, SPL, and polar graph of SPL with respect to the sampling frequency at 1 kHz respectively.

After making the piezoelectric device for $\alpha = 0.1$, 0.3, 0.5, 0.7, 0.9, and 1.0 blends, subsequently, after thermal poling at 100 °C for 5 s, we found that the sound power of $\alpha = 0.7$ and 0.9 is much increased than the other blends. The acoustic performance of the $\alpha = 0.7$ blend is the highest of those measured, whereas its polarization and dielectric properties are not superior. The 0.7 blend performs better acoustically because of its large electro-mechanical coupling associated with antiferroelectric behavior. Resultantly the increased polarization response due to its antiferroelectric behavior may eventually lead to the enhanced transduction properties. Furthermore, the 0.7 blend shows significantly lower impedance.

DISCUSSION

The transparent piezoelectric loudspeaker films were prepared by sandwiching transparent piezoelectric polymer blends between flexible PET substrates with ITO electrodes. The SPL for blends was measured. A direct correlation between SPL and the beta phase was confirmed by FTIR. We conclude percent crystallinity increases with increasing beta reflection at 1175 $\mathrm{cm^{-1}}$, correlating to an enhanced piezoelectric coefficient (d_{33}). We further conclude that after thermal poling, the polarization is enhanced, as demonstrated in an increase in beta reflection peaks. Although the *Pm*, *Pr*, and beta phase are enhanced for 0.5 to 0.9 blends, the acoustic response of the $\alpha = 0.7$ blend is higher than the rest of the system because of its higher d_{33} coefficient, enhanced *Pm* upon heating, and lower impedance. The SI of $\alpha = 0.7$ blend was also recorded as 3.98 m $\mathrm{Wm^{-2}}$, resulting in the highest SPL and SI reported in the literature. Due to their simple structure and extremely transparent characteristics, these kinds of thin films are ideal candidates to fabricate piezoelectric loudspeakers for use in smart applications.

METHODS

Material preparation

$\alpha = 0$, 0.1, 0.3, 0.5, 0.7, 0.9, and 1.0 blends were created by dissolving α grams of P(VDF-TrFE-CTFE) and 1-α grams of P(VDF-TrFE) in acetone and stirring by a magnetic stirrer at 60 °C. Solutions were kept at room temperature overnight to evaporate the residual acetone and then filtered using a 1-μm pore-sized PTFE filter. Films were produced by dispensing the polymeric solution onto glass substrates. The free-standing films were fabricated using a homemade applicator device made by scanner assembly in which the housing of scanner is used instead of an automatic applicator to fabricate the thin films. The free-standing films were then subjected to the heating furnace at 70 °C for 2 h followed by 100 °C for 1 h to improve the crystallinity. The film cross-sections were cut in a 6.5 cm × 5 cm rectangular shape to make the loudspeaker device.

Fourier transform infrared (FTIR) spectroscopy

The free-standing films were then subjected to Fourier transform spectroscopy (Bruker Optics, Model Alpha) to find the correlation between the beta phase reflections and the piezoelectric coefficient (d_{33}).

PE loops and dielectric properties

The films were characterized for PE loops using a Sawyer Tower model named Polarization Loop and Dielectric Breakdown System (Model No. PK-CPE1901). The Trek 610 C amplifier is used to amplify the output signal up to 5000 V. The samples were immersed in silicone oil to reduce the chance of short-circuiting. Impedance properties from 10 Hz to 10 kHz were measured using TA instruments.

UV-Vis spectroscopy

The percentage of transmittance and percentage of absorption of the polymer blends from 20 to 800 nm were measured with a Jenway UV Vis Spectrophotometer (Model No. 7315). The samples were held in a vertical position to detect the transmittance and absorption of the ultraviolet and visible light.

Piezoelectric coefficient (d_{33}) and piezoresponse force microscopy (PFM)

The piezoelectric coefficient (d_{33}) was measured using a quasi-static d_{33} meter (Model No. ZJ-3AN). The electromechanical properties of the piezoresponsive materials were characterized at the nanoscale using a Bruker™ PFM. The first PFM hysteresis loop was measured by applying the electric field from −10 to +10 V and another hysteresis loop was observed when applying electric field from +10 to −10 V. The samples are poled at a higher electric field (<100 $\mathrm{MVm^{-1}}$) before getting the PFM response and testing was done in poling direction to get a maximum response of electromechanical properties.

Sound pressure level (SPL) and sound intensity (SI)

SPL and SI of the free-standing sandwiched films between ITO substrates was measured with a lab-based audio detection device and captured using Smaart V7™ software. The audio is recorded in a sensitive microphone (Model No. Earldom ET-E34) placed at 1 m from the loudspeaker device. A reference microphone was also installed to reduce the pink noise. The acoustic measurements are taken in a dry environment and evaluated using the integrated impulse response method according to ISO

3382-1:2009(E) standard. The measurements were taken by applying audio signals at 1 kHz at 100 Vpp by using the UNIT-UTG1005A Function Generator. The amplification of the audio signal was done with the help of ITC Audio 120 Watt Mixer Amplifier Model T-120AP. The microphone and device setup were installed 1.5 m above the floor according to the standard in order to minimize reverberation time. SI of the device as a function of distance was measured by changing the distance between the audio detector and the loudspeaker device.

DATA AVAILABILITY

All relevant data that support the findings of this study are available from the corresponding author on request.

Received: 2 March 2021; Accepted: 21 August 2021;
Published online: 10 September 2021

REFERENCES

1. Kawai, H. The piezoelectricity of poly (vinylidene fluoride). *Jpn. J. Appl. Phys.* **8**, 975 (1969).
2. Sessler, G. M. Piezoelectricity in polyvinylidenefluoride. *J. Acoust. Soc. Am.* **70**, 1596 (1981).
3. Furukawa, T. Ferroelectric properties of vinylidene fluoride copolymers. *Phase Transit.* **18**, 143 (1989).
4. Eberle, G., Schmidt, H. & Eisenmenger, W. Piezoelectric polymer electrets. *IEEE Trans. Dielectr. Electr. Insul.* **3**, 624 (1996).
5. Yu, X., Rajamani, R., Stelson, K. A. & Cui, T. Carbon nanotube-based transparent thin film acoustic actuators and sensors. *Sens. Actuators, A Phys.* **132**, 626 (2006).
6. Wang, Y. et al. Large piezoelectricity in ternary lead-free single crystals. *Adv. Electron. Mater.* **6**, 1900949 (2020).
7. Wang, D., Yuan, G., Hao, G. & Wang, Y. All-inorganic flexible piezoelectric energy harvester enabled by two-dimensional mica. *Nano Energy* **43**, 351 (2018).
8. Wang, Y. et al. Piezo-catalysis for nondestructive tooth whitening. *Nat. Commun.* **11**, 1 (2020).
9. Chen, X. et al. Bio-inspired flexible vibration visualization sensor based on piezo-electrochromic effect. *J. Mater.* **6**, 643 (2020).
10. Sharifzadeh Mirshekarloo, M. et al. Transparent piezoelectric film speakers for windows with active noise mitigation function. *Appl. Acoust.* **137**, 90 (2018).
11. Shin, K. Y., Hong, J. Y. & Jang, J. Flexible and transparent graphene films as acoustic actuator electrodes using inkjet printing. *Chem. Commun.* **47**, 8527 (2011).
12. Tang, H., Tang, X. G., Li, M. D., Liu, Q. X. & Jiang, Y. P. Pyroelectric energy harvesting capabilities and electrocaloric effect in lead-free SrxBa1-xNb2O6 ferroelectric ceramics. *J. Alloy. Compd.* **791**, 1038 (2019).
13. Tamura, M., Yamaguchi, T., Oyaba, T. & Yoshimi, T. Electroacoustic transducers with piezoelectric high polymer films. *J. Audio Eng. Soc.* **23**, 21 (1975).
14. Ohga, J. A flat piezoelectric polymer film loudspeaker as a multi-resonance system. *J. Acoust. Soc. Jpn.* **4**, 113 (1983).
15. Lee, C. S. et al. An approach to durable poly(vinylidene fluoride) thin film loudspeaker. *J. Mater. Res.* **18**, 2904 (2003).
16. Bailo, K. C., Brei, D. E. & Grosh, K. Investigation of curved polymeric piezoelectric active diaphragms. *J. Vib. Acoust. Trans. Asme.* **125**, 145 (2003).
17. Uršič, H. & Prah, U. Investigations of ferroelectric polycrystalline bulks and thick films using piezoresponse force microscopy. *Proc. R. Soc. A: Math., Phys. Eng. Sci.* **475**, 20180782 (2019).
18. Alikin, D. O. et al. Quantitative phase separation in multiferroic Bi0.88Sm0.12FeO3 ceramics via piezoresponse force microscopy. *J. Appl. Phys.* **118**, 072004 (2015).
19. Jin, Y. et al. Studying the polarization switching in polycrystalline BiFeO3 films by 2D piezoresponse force microscopy. *Sci. Rep.* **5**, 1 (2015).
20. Tu, C. S. et al. Enhancement of local piezoresponse in samarium and manganese co-doped bismuth ferrite ceramics. *J. Alloy. Compd.* **815**, 152383 (2020).
21. Li, Q. et al. Piezoresponse force microscopy studies on the domain structures and local switching behavior of Pb(In1/2Nb1/2)O3-Pb(Mg1/3Nb2/3)O3-PbTiO3 single crystals. *J. Appl. Phys.* **112**, 052006 (2012).
22. Tripathi, A. K. et al. Multilevel information storage in ferroelectric polymer memories. *Adv. Mater.* **23**, 4146 (2011).
23. Khan, M. A., Bhansali, U. S. & Alshareef, H. N. High-performance non-volatile organic ferroelectric memory on banknotes. *Adv. Mater.* **24**, 2165 (2012).
24. Lee, C. S., Joo, J., Han, S. & Koh, S. K. Multifunctional transducer using poly (vinylidene fluoride) active layer and highly conducting poly (3,4-ethylenedioxythiophene) electrode: actuator and generator. *Appl. Phys. Lett.* **85**, 1841 (2004).
25. Xin, Y. et al. PVDF tactile sensors for detecting contact force and slip: a review. *Ferroelectrics* **504**, 31 (2016).
26. Sappati, K. K. & Bhadra, S. Piezoelectric polymer and paper substrates: a review. *Sensors* **18**, 3605 (2018).
27. Stadlober, B., Zirkl, M. & Irimia-Vladu, M. Route towards sustainable smart sensors: ferroelectric polyvinylidene fluoride-based materials and their integration in flexible electronics. *Chem. Soc. Rev.* **48**, 1787 (2019).
28. Gomes, J., Nunes, J. S., Sencadas, V. & Lanceros-Mendez, S. Influence of the β-phase content and degree of crystallinity on the piezo-and ferroelectric properties of poly(vinylidene fluoride). *Smart Mater. Struct.* **19**, 065010 (2010).
29. De Neef, A. et al. Beta phase crystallization and ferro- and piezoelectric performances of melt-processed Poly(vinylidene difluoride) Blends with Poly(methyl methacrylate) copolymers containing ionizable moieties. *ACS Appl. Polym. Mater.* **2**, 3766 (2020).
30. Shehzad, M. & Wang, Y. Structural tailing and pyroelectric energy harvesting of P(VDF-TrFE) and P(VDF-TrFE-CTFE) ferroelectric polymer blends. *ACS Omega* **5**, 13712 (2020).
31. Liu, J. H., Chen, X., Ren, Y. & Shen, Q. D. All-organic flexible logical computing system based on electrical polarization of ferroelectric polymers. *Appl. Phys. Lett.* **116**, 253301 (2020).
32. Qiu, X. et al. Fully printed piezoelectric polymer loudspeakers with enhanced acoustic performance. *Adv. Eng. Mater.* **21**, 1900537 (2019).
33. BS EN ISO 3382-1:2009. Acoustics - Measurement of room acoustic parameters. Part 1:Performance spaces. British Standard (2009).

ACKNOWLEDGEMENTS

This work was supported by the National Natural Science Foundation of China (52072178, 51790492, 11874032, and 51911530120), the Fundamental Research Funds for the Central Universities (30920041119).

AUTHOR CONTRIBUTIONS

Y.W. conceived this work and designed the experiments; M.S. and S.W performed the experiments; the data analysis was performed by M.S. and wrote the manuscript. All authors reviewed and commented on the manuscript.

COMPETING INTERESTS

The authors declare no competing interests.

ADDITIONAL INFORMATION

Supplementary information The online version contains supplementary material available at https://doi.org/10.1038/s41528-021-00121-z.

Correspondence and requests for materials should be addressed to Y. Wang.

Reprints and permission information is available at http://www.nature.com/reprints

Publisher's note Springer Nature remains neutral with regard to jurisdictional claims in published maps and institutional affiliations.